Determination of an Optimum Fictitious Air Gap and Rotor Disk Thickness for a Coreless AFPMM

Franjo PRANJIĆ, Peter VIRTIČ

Abstract: This article presents the research on the optimum distance (fictitious air gap) between permanent magnets of the coreless axial flux permanent magnet machine with a double rotor and single stator. Magnetic flux density of the permanent magnets follows the mean flux path between the opposite magnets. The size of the leakage flux depends on the axial distance between the magnets, the distance between adjacent magnets and the back iron of the rotor disks. If the fictitious air gap (clearance between opposite permanent magnets) is too large, the flux path will close through the adjacent magnet and not the opposite one. The article presents the finite element analysis of the magnetic flux density between the permanent magnets mounted on the rotor disks where the fictitious air gap thickness was set as a variable to determine the maximum clearance. Connection between bending (pull) forces of rotor disks and fictitious air gap thickness is also presented with the mechanical stress analysis of rotor disks.

Keywords: Axial Flux Permanent Magnet Machine (AFPMM); Mechanical Stress Analysis (MSA); optimum fictitious air gap thickness; rotor disk thickness

1 INTRODUCTION

Axial flux permanent magnet machines (AFPMM) are growing more and more popular lately due to their compactness, a high degree of reliability, efficiency, simple construction and high power density [1-7]. As shown in Fig.1, this type of machines, which are also called "disk" type machines, have various topologies:

- single-sided (one stator and one rotor)
- double-sided (single stator – double rotor or single rotor – double stator)
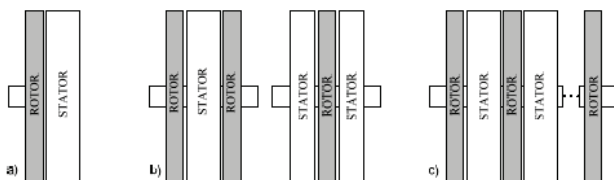- multistage (multiple rotors and stators).

Figure 1 Basic topologies of AFPMM: a) single-sided, b) double-sided, c) multistage

All of the above-mentioned topologies can be constructed with or without iron cores (coreless) and with surface mounted or buried PMs. Low power PM machines are usually coreless and have surface mounted PMs [1].

Each machine topology has its own strengths and weaknesses. Topologies without stator cores are used for low and medium power generators and have the advantages, such as absence of cogging torque, linear torque-current characteristics, high power density and compact construction.

Due to the absence of the stator core losses, this type of generators can operate with a higher efficiency than the conventional generators [2-5].

This article presents the determination of the optimum size of the fictitious air gap thickness for AFPMM with two external rotors and one internal coreless stator (without ferromagnetic material as the copper windings are held together in position by using a composite material of epoxy resin), using numerous finite element analysis (FEA) simulations in Ansys Maxwell 3D software.

As the name itself states, the axial flux machine requires magnetic flux to pass in the axial direction. If the thickness of fictitious air gap is too large (usually this means large stator thickness), the magnetic flux path will close through the air and into the same PM or through the adjacent PM. Consequently, a very small portion of magnetic flux will pass in axial direction (large leakage flux), and the machine will produce smaller torque and electromotive force (EMF).

Finding an optimum thickness of fictitious air gap allows the highest possible portion of magnetic flux to pass from PM on one rotor disk to the PM on opposite rotor disk with minimal flux leakage.

Since the magnetic flux density in the fictitious air gap is one of the key values for calculation of static torque, back EMF and pull forces between opposite rotor disks, the derivation of equation for magnetic flux density in the fictitious air gap is presented with a magnetic equivalent circuit (MEC).

The relation between magnetic flux density and back EMF is presented with Eq. (1) and Eq. (2) [3]:

$$e = -N \frac{\mathrm{d}\Phi}{\mathrm{d}t} \tag{1}$$

$$\Phi = \iint_S B \mathrm{d}S \tag{2}$$

where B is the magnetic flux density, N the number of turns in a coil, e the EMF, $\mathrm{d}\Phi/\mathrm{d}t$ the time variation of magnetic flux within the coil, $\mathrm{d}S$ the integration surface, and Φ the magnetic flux.

The mechanical stress analysis (MSA) of rotor disks is presented since magnetic pull forces and the thickness of rotor disks depend on the air gap flux density.

The MSA has been introduced in several publications. In [8], the authors present the MSA for a high speed AFPMM, where they analyze the stress level of the rotor disks due to high-speed rotation, using three-dimensional finite element method (3D FEM). Fei et al. present simplified 2D and 3D FEM for analysis and design of rotor disks of high-speed AFPM generators in [9]. Rani et al. present a computational method of rotor stress analysis for conventional rotors using J-MAG software in [10]. In [11], the authors present the structural analysis of low-speed axial-flux permanent-magnet machines. Timoshenko

derived the equations for bending circular plates in [12], and in [13], Young and Budynas present various scenarios for different loads on circular plates.

The link between electromagnetic and structural designs is Maxwell stress. To determine the air gap flux density, classical analysis of magnetic equivalent circuits can be used, hence the Maxwell stress is given by:

$$q = \frac{B_\mathrm{d}^2}{2\mu_0} \tag{3}$$

where q (Pa) is the Maxwell stress, B_d the axial component of air gap flux density and μ_0 the permeability of vacuum [10].

Maxwell stress is represented by the magnetic pull force acting between the rotor disks and can be calculated as magnetic pressure multiplied by active surface area of all PMs (SPM) as shown in [1]:

$$F = \frac{B_\mathrm{d}^2}{2\mu_0}\left(S_\mathrm{PM}\right) \tag{4}$$

$$S_\mathrm{PM} = \alpha_i \frac{\pi}{4}\left(D_\mathrm{out}^2 - D_\mathrm{in}^2\right) \tag{5}$$

$$\alpha_i = \frac{\alpha_\mathrm{PM} 2p}{360} \tag{6}$$

where F is the pull force between opposite PMs, α_PM the angle of PMs, α_i the coefficient, which is calculated as angle of PMs multiplied by the number of PMs per rotor disk (poles) and divided by 360 degrees, and D_out and D_in are the outer and inner diameters of PMs, respectively.

In [13], the authors present equations for various types of loads on a circular plate where the case suitable for rotor disks of AFPMM with surface mounted PMs is presented in Fig. 2.

Equations for deflection calculations are [12-14]:

$$y_\mathrm{a} = M_\mathrm{rb}\frac{a_\mathrm{r}^2}{D}C_2 + Q_\mathrm{b}\frac{a_\mathrm{r}^3}{D}C_3 + q\frac{a_\mathrm{r}^4}{D}L_{11} \tag{7}$$

$$M_\mathrm{rb} = \frac{-qa_\mathrm{r}^2}{C_8}\left(\frac{C_9}{2a_\mathrm{r}b_\mathrm{r}}\left(a_\mathrm{r}^2 - r_0^2\right) - L_{17}\right) \tag{8}$$

$$Q_\mathrm{b} = \frac{q}{2b_\mathrm{r}}\left(a_\mathrm{r}^2 - r_0^2\right) \tag{9}$$

$$C_2 = \frac{1}{4}\left(1 - \left(\frac{b_\mathrm{r}}{a_\mathrm{r}}\right)^2\left(1 + 2\ln\left(\frac{a_\mathrm{r}}{b_\mathrm{r}}\right)\right)\right) \tag{10}$$

$$C_3 = \frac{b_\mathrm{r}}{4a_\mathrm{r}}\left(\left(\left(\frac{b_\mathrm{r}}{a_\mathrm{r}}\right)^2 + 1\right)\ln\left(\frac{a_\mathrm{r}}{b_\mathrm{r}}\right) + \left(\frac{b_\mathrm{r}}{a_\mathrm{r}}\right)^2 - 1\right) \tag{11}$$

$$C_8 = \frac{1}{2}\left(1 + v + (1-v)\left(\frac{b_\mathrm{r}}{a_\mathrm{r}}\right)^2\right) \tag{12}$$

$$C_9 = \frac{b_\mathrm{r}}{a_\mathrm{r}}\left(\frac{1+v}{2}\ln\left(\frac{a_\mathrm{r}}{b_\mathrm{r}}\right) + \frac{1-v}{4}\left(1 - \left(\frac{b_\mathrm{r}}{a_\mathrm{r}}\right)^2\right)\right) \tag{13}$$

$$D = \frac{Et^3}{12(1-v^2)} \tag{14}$$

$$L_{17} = \frac{1}{4}\left(1 - \frac{1-v}{4}\left(1 - \left(\frac{r_0}{a_\mathrm{r}}\right)^4\right) - \left(\frac{r_0}{a_\mathrm{r}}\right)^2\left(1 + (1+v)\ln\left(\frac{a_\mathrm{r}}{r_0}\right)\right)\right) \tag{15}$$

$$L_{11} = \frac{1}{64}\left(1 + 4\left(\frac{r_0}{a_\mathrm{r}}\right)^2 - 5\left(\frac{r_0}{a_\mathrm{r}}\right)^4 - 4\left(\frac{r_0}{a_\mathrm{r}}\right)^2\left(2 + \left(\frac{r_0}{a_\mathrm{r}}\right)^2\right)\ln\left(\frac{a_\mathrm{r}}{r_0}\right)\right) \tag{16}$$
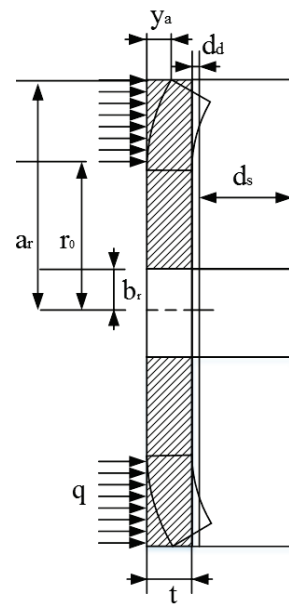
Figure 2 Circular plate model

where: y_a is the deflection of the rotor disk, M_rb the bending moment, a_r the outer radius of the rotor disk, b_r the inner radius of the rotor disk, r_0 the radial location of unit line loading or start of a distributed load, D the stiffness factor of the material, Q_b the unit shear force (force per unit of circumferential length), and q the magnetic pressure (or Maxwell stress). C_2, C_3 and C_9 are the plate constants dependent upon the ratio a/b, and L_{11} and L_{17} are the loading constants dependent upon the ratio a/r_0. v is the Poisson's ratio, D a constant termed the "flexural stiffness" or "flexural rigidity", E the elastic module of the material used, t the thickness of the rotor disk.

Eq. (3) - Eq. (16) are used to determine the optimum rotor disk thickness through deflection of rotor disks, based on the axial component of magnetic flux density.

Finally, the conclusions of the research are presented, such as the direct link between the thickness of fictitious air gap, deflection of rotor disks and rotor disk thickness through magnetic flux density in the fictitious air gap.

In this article, a direct link between magnetic flux density and optimum thickness of fictitious air gap is presented for the first time as well as a modified equation for deflection of rotor disks together with a simple

methodology for determining the optimum thickness of the fictitious air gap.

2 METHODS
2.1 Analytical Determination of Magnetic Flux Density in the Fictitious Air Gap

The AFPMM considered in this article is a double-sided AFPMM with two external rotors and one internal coreless stator. It was analysed in [3] and optimized in [14] by using evolutionary optimization with a genetic algorithm and an analytical evaluation of objective functions. Also in [15] the rotor disk thickness was analysed in relation to the magnitudes of magnetic flux density.

Figure 3 Rotor and Permanent magnets of a coreless AFPMM

Tab. 1 shows the data relevant to this study, and Fig. 3 shows the rotor disks with surface mounted PMs.

Table 1 geometry and parameters of analysed AFPMM)

Symbol	Quantity	Value/Unit
R	Rotor disk radius	150 mm
t	Rotor disk thickness	7 mm
PM	Type of PM	NdFeB
h_{PM}	Permanent magnet thickness	5 mm
τ_{PM}	Magnetic pitch	25°
R_{inPM}	Inner radius of PM	80 mm
R_{outPM}	Outer radius of PM	150 mm
B_r	Remanent magnetic flux density	1,22 T
τ_p	Pole pitch	36°
p	Number of pole pairs	5
μ_r	Relative recoil permeability	1,0704
I	Rated current	10 A
k_w	Winding factor	0,966

In Fig. 4 the fictitious air gap is the mechanical clearance between the opposite permanent magnets, where d is the fictitious air gap, d_s the stator thickness, d_d the air gap thickness, and l_{AM} the distance between adjacent magnets.

Path 1 represents the mean magnetic flux. The magnetic flux that does not follow the mean flux path (path 1) is considered to be leakage flux and represented by path 2 (magnet to air) and path 3 (magnet to magnet).
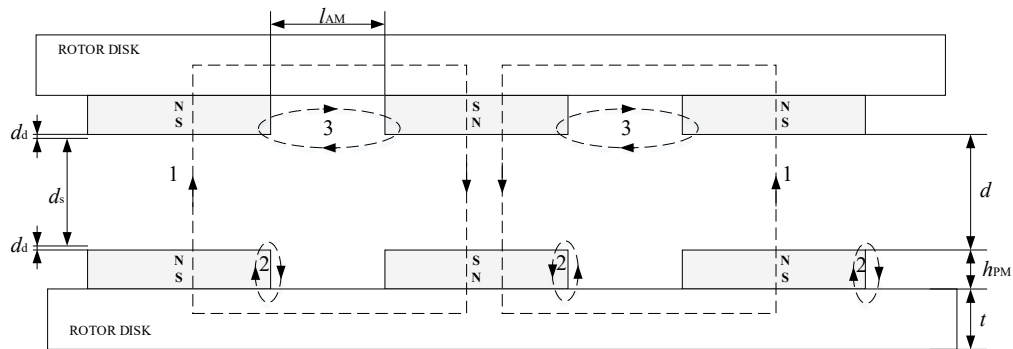
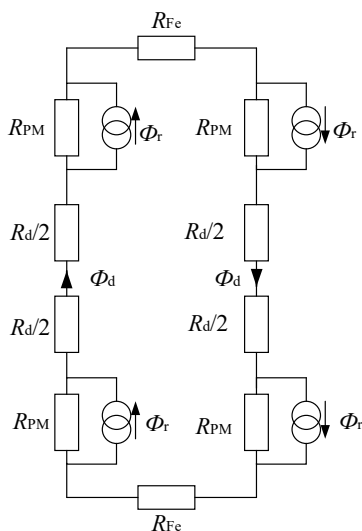**Figure 4** Sectional view of AFPMM

Figure 4 Magnetic equivalent circle of coreless AFPMM

Fig. 5 shows the equivalent magnetic circuit of the coreless AFPMM, where R_{Fe} is the reluctance of the iron disks, R_{PM} is the reluctance of the permanent magnets, R_d

is the reluctance of the fictitious air gap, and Φ_r and Φ_d are the magnetic flux through the PMs and through the fictitious air gap respectively.

In an ideal situation, the magnetic flux would follow the mean flux path, but in reality, there is also the leakage flux, which can be reduced (for coreless AFPMM) by using measures listed in [16]:
- the axial length of the air gap has to be smaller than double thicknesses of the PMs in the magnetization direction ($d < 2h_{PM}$),
- the distance between neighboring PMs on the same disk has to be larger than the fictitious air gap ($l_{AM} > d$).

These measures work under the assumption that the magnetic flux will always follow the shortest path from one pole to another.

Since this type of AFPMM has no ferromagnetic stator core, a simplified MEC (magnetic equivalent circuit) is defined by neglecting iron rotor yoke reluctance due to the high permeability of steel, where magnets are represented by a flux source with parallel reluctance defined by their nominal magnetization values and geometry.
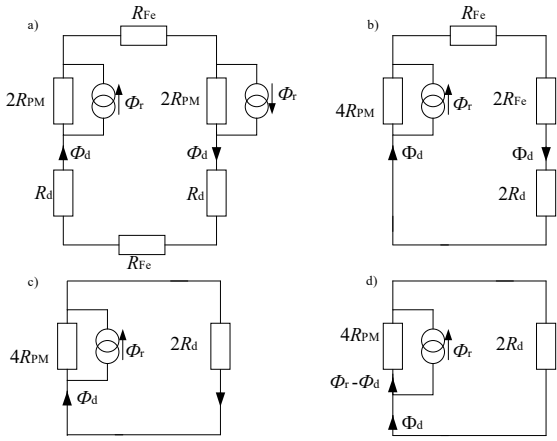
Figure 5 Simplifications of the magnetic network model of coreless AFPMM

Using the second Kirchhoff law in Fig. 6d, the equation for magnetic flux density in the middle of the air gap (axial component) can be determined. The saturation of rotor back iron is also neglected since the relative permeability of steel is considered infinite compared to the permeability of air [8].

Using the relation from Fig. 6d under assumption that the area of PMs and air gap are equal, the equation for calculating the magnetic flux density can be written as:

$$B_d A_d = \frac{\dfrac{h_{PM}}{\mu_0 \mu_r A_{PM}} B_r A_{PM}}{\dfrac{h_{PM}}{\mu_0 \mu_r A_{PM}} + 0,5 \dfrac{d}{\mu_0 A_d}}$$

$$B_d = \frac{\dfrac{h_{PM}}{\mu_0 \mu_r} B_r}{\dfrac{h_{PM}}{\mu_0 \mu_r} + 0,5 \dfrac{d}{\mu_0}} = \frac{h_{PM} B_r}{h_{PM} + 0,5 d \mu_r} \qquad (17)$$

$$B_d = \frac{B_r}{1 + \dfrac{0,5 d \mu_r}{h_{PM}}}$$

Mean flux path from one pole to the other is through the fictitious air gap (d), which represents the stator thickness (d_s) and the thickness of the two air gaps ($2d_d$). The equation for magnetic flux density in the air gap takes its final form:

$$B_d = \frac{B_r}{1 + \dfrac{0,5(d_s + 2d_d)\mu_r}{h_{PM}}} \qquad (18)$$

where B_r is permanent magnetic flux density in the air gap, h_{PM} the permanent magnet thickness and μ_r the relative recoil permeability of the PMs.

Fig. 4 - Fig. 6 and Eq. (18) show that the fictitious air gap has a significant influence on the magnetic flux density. Thicker air gap means smaller magnetic flux density in axial direction.

2.2 Determination of Optimum Fictitious Air Gap Thickness

AFPMM model is constructed using Ansys Maxwell 3D software and the data from Tab. 1. Fig. 7a shows the starting model of the study, which consists of two 7 mm thick rotor disks with 10 PMs mounted on each one. Between them, there is a 100 mm air gap with 5 mm layers. Each air gap layer represents a new FEA simulation of air gap flux density (i.e., Fig. 7b shows the meshed model with 55 mm fictitious air gap), which is analyzed on a line that runs through both rotor disks, all the air gaps and 2 PMs. The line is drawn through the centre of the PMs on the average radius, as shown in Fig. 8.

FEA simulations are performed for the thickness of fictitious air gap from 5 mm to 100 mm with 5mm steps, which in total represents 20 simulations. The result of each simulation is the axial component of the magnetic flux density on the centerline (Fig. 8) between opposite PMs.
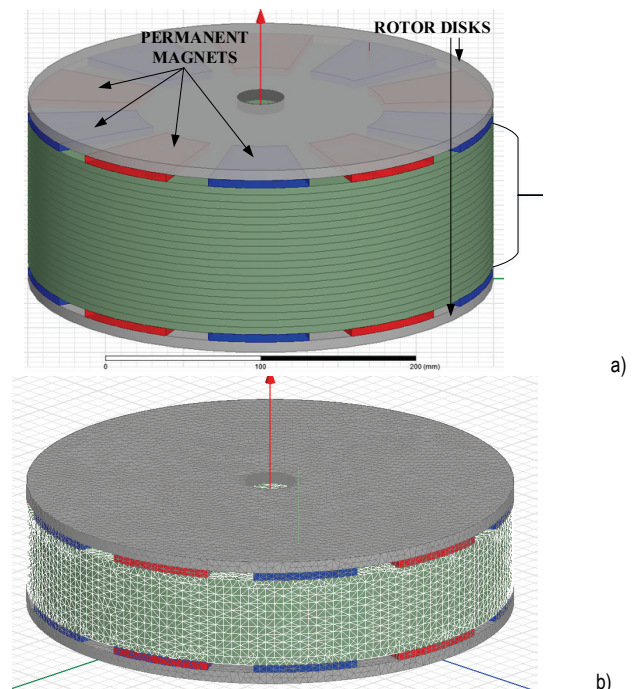

Figure 7 AFPMM model (a-starting model with 100mm fictitious air gap, b-meshed model with 55 mm fictitious air gap)
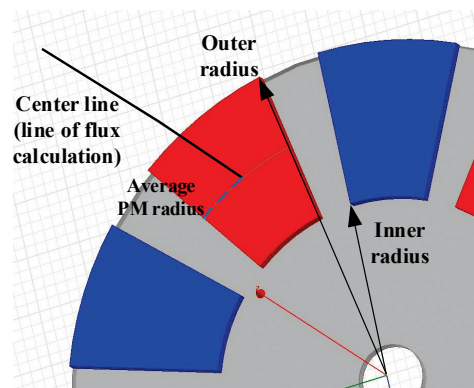

Figure 8 Dimensions of the PMs and the centreline

2.3 Mechanical Stress Analysis of Rotor Disks

Deflection of rotor disks is calculated with Eq. (3) and Eq. (6) - Eq. (16) together with the magnetic flux densities

in the middle of the fictitious air gap from Tab. 2. Based on the results, the optimum disk thickness can be determined in order to reduce the weight of the machine, since rotor disks represent around 40% of total weight of the machine [1].

Deflection of rotor disks is caused by the magnetic pressure which results from the PMs. For that reason, the equation for calculating deflection of rotor disks (Eq. (7)) is modified with Eq. (6), since the authors in [12] and [13] derived the equations for bending circular plates with uniformly distributed loads. A new equation for deflection of rotor disks takes the form of Eq. (19):

$$y = \alpha_i y_a \tag{19}$$

where α_i is the angle of PMs multiplied by the number of PMs per rotor disk (poles) and divided by 360 degrees, and ya is the deflection derived in [12].

The MSA is performed for the 7 mm thickness of rotor disk using analytically calculated (using Eq. (18)) and FEA gained axial component of magnetic flux density in the middle of the fictitious air gap.

Pull force between opposite rotor disks is calculated using Eq. (4) and Eq. (5) for analytically calculated and FEA gained magnetic flux density in the middle of the fictitious air gap. In addition, the deflection of rotor disks is determined analytically with Eq. (19) and with FEA, using Solid works software. In total, four deflections of rotor disks are calculated and presented.

3 RESULTS AND DISCUSSION
3.1 Determination of Optimum Fictitious Air Gap Thickness

Fig. 9 presents the results of FEA simulations for the thicknesses of the fictitious air gap from 5 mm to 100 mm with 5 mm steps. It shows that sectional magnets with 5 mm thickness have the optimum fictitious air gap up to 20 mm thickness since there is negligible difference in the axial component of magnetic flux density in the middle of the fictitious air gap and near the PMs. For larger air gaps, these values start to differentiate, the larger the air gap, the larger the difference.
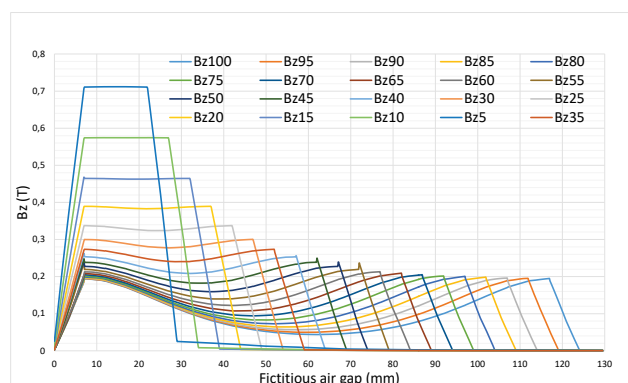

Figure 9 Magnetic flux density in axial direction for all air gaps

The values of axial component of magnetic flux density near the PMs and in the middle of the fictitious air gaps are respectively marked as B_{z_max} and B_{z_min} in Fig. 10, which shows a single value waveform for 55 mm air gap thickness.
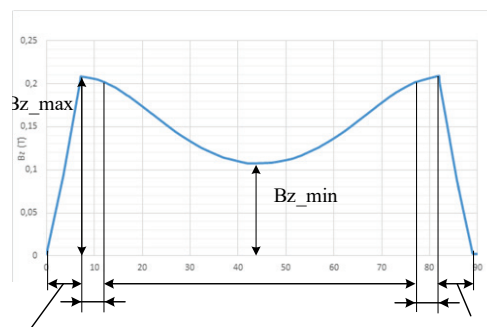

Figure 10 Positions of maximum and minimum axial component magnetic flux density

Tab. 2 and Fig. 11 show maximum and minimum values of magnetic flux density in axial direction between the PMs.

Table 2 Axial component of magnetic flux density in the fictitious air gap (FEA)

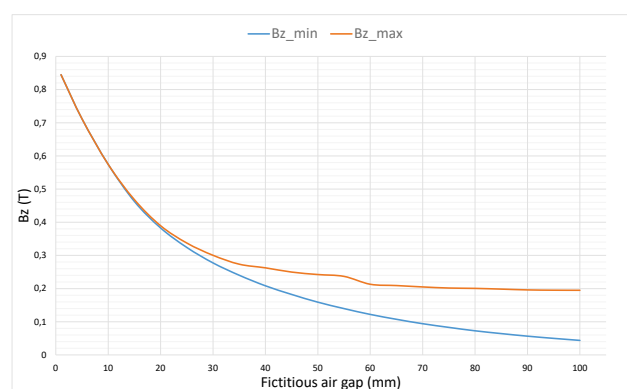| Fictitious air gap thickness d (mm)	B_{z_min} (T)	B_{z_max} (T)	Difference (%)
1	0,8448	0,8448	0
5	0,711825	0,711825	0
10	0,574517	0,574517	0
15	0,462765	0,468164	1,15323
20	0,382824	0,389489	1,71122
25	0,324058	0,337344	3,93841
30	0,277382	0,300347	7,64616
35	0,24023	0,273567	12,1860
40	0,208391	0,262567	20,6332
45	0,182382	0,249802	26,9894
50	0,159055	0,242391	34,3808
55	0,139678	0,236783	41,0101
60	0,122135	0,213067	42,6777
65	0,107387	0,209165	48,6592
70	0,094125	0,205	54,0854
75	0,083002	0,201669	58,8425
80	0,072718	0,200631	63,7554
85	0,06430451	0,198421343	67,5919
90	0,056541924	0,196034607	71,1572
95	0,049904851	0,195151265	74,4276
100	0,043782218	0,194908347	77,5370

Figure 11 B_{z_max} and B_{z_min} in axial direction between the PMs

The optimum thickness of fictitious air gap is selected in such a way that there is minimum flux leakage, which means that the magnetic flux is following the mean flux path in full.

Tab. 2 shows that the values of axial component of magnetic flux density do not change for 10 mm thickness of fictitious air gap, which means that there is no leakage flux. Negligible change of axial component of magnetic flux density can be seen for 20 or even 25 mm thickness.

The data are graphically shown in Fig. 11, and it is clear that the magnetic flux density changes exponentially in relation to the thickness of fictitious air gap.

Results in Tab. 2 also confirm the measure for reducing the flux leakage (axial length of the air gap has to be smaller than double thicknesses of the PMs in the magnetization direction).

3.2 Mechanical Stress Analysis of Rotor Disks

Pull forces between opposite rotor disks are calculated using Eq. (4) and Eq. (5) for analytically and FEA gained axial component of magnetic flux density and are presented in Tab. 3 and Fig. 12.

Table 3 Pull forces on rotor disks due to analytically and with FEA gained B_z

| Fictitious air gap thickness d (mm)	B_z (T) FEA	B_z (T) Analytical	F_Z (N) FEA	F_Z (N) Analytical
5	0,7118	0,7947	7081,4	8826
10	0,5745	0,5893	4613	4853
15	0,4628	0,4682	2993	3064
20	0,3828	0,3884	2048	2109
25	0,3241	0,3319	1467,6	1539,4
30	0,2774	0,2897	1075,3	1173
35	0,2402	0,257	806,5	923,4
40	0,2084	0,231	607	746
45	0,1824	0,2097	465	615
50	0,1591	0,1921	353,6	515,6
55	0,1397	0,1771	272,7	483,5
60	0,1221	0,1644	208,5	377,6
65	0,1074	0,1533	161,2	328,5
70	0,0941	0,1437	123,82	288,4
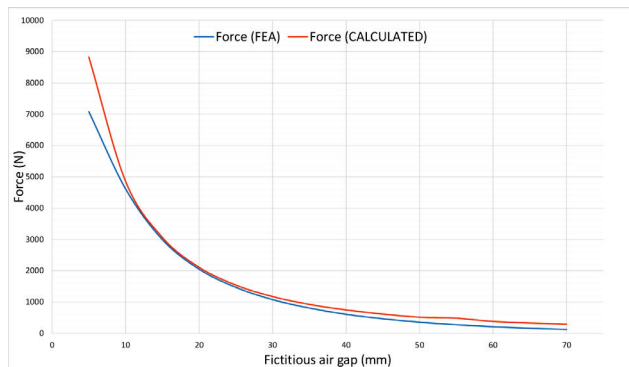
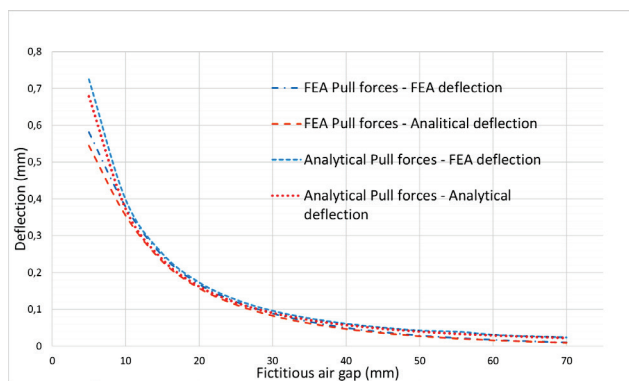**Figure 12** Analytically and FEA gained pull forces

Figure 13 Deflection of rotor disks

Deflection of rotor disks is calculated with Eq. (19) and determined with FEA, using SolidWorks software. In total, four deflections of rotor disks are calculated and presented in Tab. 4 and Tab. 5.

Fig. 13 shows the deflections of rotor disks for four scenarios. The first scenario is based on the FEA gained pull force, where force is calculated using Eq. (4) and FEA gained axial component of magnetic flux density (B_z) and simulated with FEA, using Solidworks software.

For second scenario, Eq. (19) is used for calculating deflection of rotor disks instead of FEA.

Table 4 Deflection of rotor disks for FEA gained pull forces

Fictitious air gap thickness d (mm)	Deflection of rotor disks (mm) FEA	Deflection of rotor disks (mm) Analytical
5	0,5817	0,54475
10	0,3788	0,35486
15	0,2459	0,23023
20	0,1684	0,15756
25	0,1208	0,1129
30	0,08874	0,082719
35	0,06655	0,062044
40	0,04987	0,046688
45	0,03821	0,035761
50	0,02909	0,027198
55	0,02243	0,020975
60	0,01725	0,016037
65	0,01323	0,012398
70	0,01019	0,0095249

For third and fourth scenarios analytically calculated pull forces are used.

Table 5 Deflection of rotor disks for analytically gained pull forces

Fictitious air gap thickness d (mm)	Deflection of rotor disks (mm) FEA	Deflection of rotor disks (mm) Analytical
5	0,7255	0,67898
10	0,3985	0,37335
15	0,2518	0,23567
20	0,1734	0,16218
25	0,1265	0,11843
30	0,09613	0,090229
35	0,07592	0,071009
40	0,0613	0,057368
45	0,05053	0,047276
50	0,0424	0,039674
55	0,03977	0,03372
60	0,03106	0,029057
65	0,02703	0,025266
70	0,02383	0,0222

Deflection of rotor disks is important for optimum thickness selection of rotor disk, which is selected based on the maximum allowed deflection (y). When the geometry of rotor disks and PMs is defined (inner radius, outer radius, shaft and PM thickness) as well as maximum deflection, the thickness of fictitious air gap and corresponding axial component of magnetic flux density can be found in Tab. 2, Tab. 4 and Tab. 5. Once the corresponding axial component of magnetic flux density is obtained, Eq. (7), Eq. (14) and Eq. (19) can be rearranged to obtain the optimum disk thickness of rotor disks, where q, M_{rb} and Q depend on the axial component of magnetic flux density.

$$t = \sqrt[3]{\frac{\alpha_i 12\left(1-v^2\right)\left(M_{rb} a_r^2 C_2 + Q_b a_r^3 C_3 + q a_r^4 L_{11}\right)}{Ey}} \tag{20}$$

Deflection of rotor disks (among other factors) depends on the stiffness factor (Eq. (14)), and the latter depends on the selected material and its thickness. Eq. (20) shows the derived thickness of rotor disks from Eq. (7), Eq. (14) and Eq. (19) for the purpose of direct calculation of rotor disk thickness.

3.3 Validation of the Methodology

Electromotive force (EMF) of the prototype described in Tab. 1 was measured at 600 rpm, using the Yokogawa WT1800 Power Quality Analyser.

The results are shown in Tab. 6 and the measuring equipment in Fig. 14.

Table 6 Measured RMS Values of the Back EMF

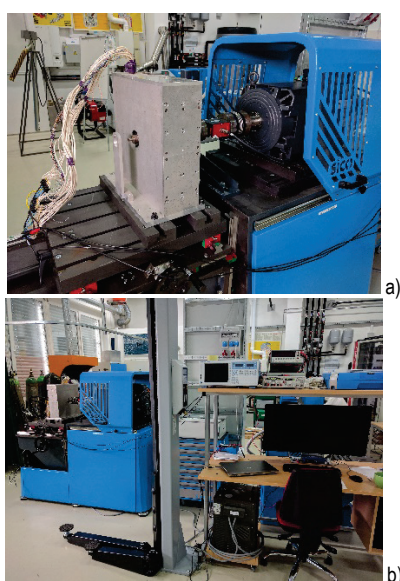| E_1	E_2	E_3	E_{avg}
33,63	33,7	34	33,777

Figure 14 Measuring equipment: (a) Prototype AFPMM mounted on the measuring table, (b) complete view of measuring equipment

Analytical results are obtained by inputting the FEA gained axial component of magnetic flux density and the data from Tab. 1 into Eq. (21) and Eq. (22) [1].

$$\Phi = \alpha_i B_d \frac{\pi}{8p}\left(D_{out}^2 - D_{in}^2\right) \tag{21}$$

$$E = \pi\sqrt{2}\, fNk_w \Phi \tag{22}$$

Magnetic flux (Φ) can be calculated with Eq. (21) and RMS value of EMF with Eq. (22), where α_i is the angle of PMs multiplied by the number of PMs per rotor disk (poles) and divided by 360 degrees (α_i also represents the magnet pitch to pole pitch factor), B_d the axial component of magnetic flux density, and D_{out} and D_{in} are the outer and inner diameters of PMs, respectively. f is the network frequency (50 Hz), N the number of turns in a coil, k_w the winding factor, h the number of rotor disks and I the rated current.

The calculations are performed for B_d in the middle of 17 mm fictitious air gap (as the prototype machine is constructed; 15 mm stator + 2×1 mm air gap) and the results are shown in Tab. 7.

Table 7 Verification of the methodology calculated results

Magnetic flux Φ (Wb)	B_d (T)	RMS value of Back EMF (V)
0,001513	0,430753	32,46766

Comparison of the average RMS value of measured EMF and the calculated value shows that the difference between them is less than 4%.

4 CONCLUSION

Derivation of Eq. (18) shows the link between the axial component of magnetic flux density and the thickness of fictitious air gap. The value changes exponentially with the fictitious air gap thickness as shown in Fig. 11.

Since deflection of rotor disks (due to magnetic pull forces between opposite disks) is directly connected to the axial component of magnetic flux density, the deflection of rotor disks also changes exponentially. By changing a well-known set of equations for circular plate deflection, a new equation for deflection of rotor disks is formed. Fig. 13 shows that the equations for deflection of rotor disks and axial component of magnetic flux density are quite accurate for initial dimensioning of rotor disk thickness.

The article presents a new and simple methodology for finding an optimum range of fictitious air gap thicknesses based on axial component of magnetic flux density of the PMs.

Since axial component of magnetic flux density is directly linked to magnetic pull forces, a modified equation for rotor disks deflection was derived and presented. Fig. 13 validates that equation is suitable for initial dimensioning of rotor disks, and compared to FEA analysis the accuracy is above 90%, depending on the thickness of the fictitious air gap.

The methodology is also verified through measurement of the effective EMF value of the prototype machine. The results show that the methodology described in this article is accurate since calculated and measured RMS value of EMF differentiates less than 4%.

5 REFERENCES

[1] Gieras, J. F., Wang, R. J., & Kamper M. J. (2004). *Axial Flux Permanent Magnet Brushless Machines*. Dordrecht: Kluwer Academic Publishers.

[2] Chan, T. F. & Lai, L. L. (2007). An Axial-Flux Permanent-Magnet Synchronous Generator for a Direct-Coupled Wind-Turbine System. *IEEE Trans. Energy Convers., 22*(1), 86-94. https://doi.org/10.1109/TEC.2006.889546

[3] Virtic, P., Pisek, P., Marcic, T., Hadziselimovic, M., & Stumberger, B. (2008). Analytical Analysis of Magnetic Field and Back Electromotive Force Calculation of an Axial-Flux Permanent Magnet Synchronous Generator with Coreless Stator. *IEEE Transactions on Magnetics*, *44*(11), 4333-4336. https://doi.org/10.1109/TMAG.2008.2001528

[4] Wang, X. & Xiao, K. (2009). Analysis for Magnetic Field in the Air Gap of the Wheel Multi-disc Coreless Permanent Magnet Synchronous Motor. *Int. Conf. Electrical Machines and Systems*, 1-4. https://doi.org/10.1109/ICEMS.2009.5382983

[5] Pinilla, M. & Martinez, S. (2011). Selection of main design variables for low-speed permanent magnet machines devoted to renewable energy conversion. *IEEE Trans. Energy Convers., 26*(3), 940-945. https://doi.org/10.1109/TEC.2011.2157161

[6] Kumar, S., Lipo, T. A., & Kwon, B. (2016). A 32,000 rev/min axial flux permanent magnet machine for energy storage with mechanical stress analysis. *IEEE Trans. Magn.*, *52*(7), 1-4. https://doi.org/10.1109/TMAG.2015.2512939

[7] Hatami, H., Bagher, M., Sharifian, B., & Sabahi, M. (2013). A New Design Method for Low-Speed Torus Type AFPM Machine for Hev Applications. *IJRET International Journal of Research in Engineering and Technology, 2*(12), 396-406. Retrieved from http://esatjournals.net/ijret/2013v02/i12/IJRET20130212067.pdf

[8] Pyrhonen, J., Jokinen T., & Hrabovcova V. (2009). *Design of Rotating Electrical Machines*. Wiley and Sons, Wiley online.

[9] Fei, W., Luk, P. C. K., & El-Hasan, T. S. (2011). Rotor integrity design for a high-speed modular air-cored axial-flux permanent-magnet generator. *IEEE Trans. Ind. Electron., 58*(9), 3848-3858. https://doi.org/10.1109/TIE.2011.2106097

[10] Rani, J. A., Sulaiman, E., Omar, M. F., Ahmad, M. Z., & Khan, F. (2015). Computational Method of Rotor Stress Analysis for Various Flux Switching Machine Using J-MAG. *IEEE Student Conference on Research and Development (SCOReD)*, 721-726. https://doi.org/10.1109/SCORED.2015.7449433

[11] Mueller, M. A., McDonald, A. S., & Macpherson, D. E. (2005). Structural analysis of low-speed axial-flux permanent-magnet machines. *IEE Proceedings-Electric Power Appl.*, *152*(6), 1417-1426. https://doi.org/10.1049/ip-epa:20050227

[12] Timoshenko, S. (1987), *Theory of Plates and Shells*. New York, NY: McGraw-Hill Book Company.

[13] Young, W. C. & Budynas, R. G. (2002). *Roark's Formulas for Stress and Strain*. New York, NY: McGraw-Hill Book Company.

[14] Virtic, P., Vražic, M., & Papa, G. (2016). Design of an Axial Flux Permanent Magnet Synchronous Machine Using Analytical Method and Evolutionary Optimization. *IEEE Trans. Energy Convers., 31*(1), 150-158. https://doi.org/10.1109/TEC.2015.2477319

[15] Virtic, P. (2012). Analysis of rotor disk thickness in coreless stator axial flux permanent magnet synchronous machine. *Przegląd Elektrotechniczny, 33*(12), 12-15. Retrieved from http://pe.org.pl/articles/2012/12b/4.pdf

[16] Mbidi, D. N. (2001). *Design and Evaluation of a 300 kW Double Stage Axial-Flux Permanent Magnet Generator*. Thesis (MScEng)-Stellenbosch University. Retrieved from http://hdl.handle.net/10019.1/52177

Contact information:

Franjo PRANJIĆ, Master of Energy Technology
University of Maribor, Faculty of Energy Technology,
Hočevarjev trg 1, 8270 Krško, Slovenia
franjo.pranjic@um.si

dr. **Peter VIRTIČ**
University of Maribor, Faculty of Energy Technology,
Hočevarjev trg 1, 8270 Krško, Slovenia
peter.virtic@um.si